

Article

Directional Suppression of Monotone Noises with A Parametric Array Loudspeaker

Han Wang^{1,2,*}, Jingxiao Zhang¹, Lin Gan^{3,*} and Yu Liu^{1,2}

¹ School of Microelectronics, Tianjin University, Tianjin 300072, China; zhangjingxiao_hh@tju.edu.cn (J.Z.); liuyu@tju.edu.cn (Y.L.)

² International Institute for Innovative Design and Intelligent Manufacturing of Tianjin University in Zhejiang, Shaoxing 312077, China

³ College of Intelligence and Computing, Tianjin University, Tianjin 300072, China

* Correspondence: yaohua-wh@163.com (H.W.); ganlin@tju.edu.cn (L.G.)

Abstract: Monotone noises at high decibels have been identified as a main cause of degradation in people’s mental health. This paper proposes a directional monotone noise reduction method to suppress spatially localized single-frequency noises. The system is designed based on a feedforward active noise control (ANC) structure by implementing filtered-x least mean square (FxLMS) algorithms. Compared with traditional ANC methods, our system employs a parametric array loudspeaker (PAL) as the active noise-canceling source with high audio directivity for directional noise suppression. The system monitors the ambient monotone noise and implements the ANC algorithm in real-time through a software-based platform operating on a generic personal computer (PC). Experimental measurements demonstrate an 8 dB reduction of different monotone noises at a 260 cm distance from the active source. Compared with traditional ANC methods with a voice coil loudspeaker (VCL) as the noise-canceling source, our PAL-based system achieves similar noise suppression performance with a 5.8 times improvement in the source-to-target distance and 64% reduction in the -3 dB audio main lobe beam width. The results prove the advantage of introducing PALs as active-noise-canceling sources for monotone noise suppression with a cost-effective enhancement in operating distances and noise control directivities.

Keywords: parametric array loudspeaker; active noise control; filtered-x least mean square; directional noise suppression; monotone noise



Citation: Wang, H.; Zhang, J.; Gan, L.; Liu, Y. Directional Suppression of Monotone Noises with A Parametric Array Loudspeaker. *Appl. Sci.* **2023**, *13*, 6868. <https://doi.org/10.3390/app13126868>

Academic Editor: Masayuki Takada

Received: 4 May 2023

Revised: 31 May 2023

Accepted: 2 June 2023

Published: 6 June 2023



Copyright: © 2023 by the authors. Licensee MDPI, Basel, Switzerland. This article is an open access article distributed under the terms and conditions of the Creative Commons Attribution (CC BY) license (<https://creativecommons.org/licenses/by/4.0/>).

1. Introduction

It is well-recognized that long-term exposure to environmental noises can induce multiple health issues [1] such as hearing loss [2], cardiovascular diseases [3], and mental-related issues such as stress and impairment of cognition [4]. Among different noise types categorized by spectrum characteristics, monotone noise is similar to human tinnitus sensation and can cause emotional and cognitive disorders that lead to behavioral disability [5]. Hence, eliminating monotone noise is a crucial task in environmental noise management.

Noise reduction schemes can be categorized as either controlling the noise source, handling the noise propagation path, or isolating the receiver. In practice, passive noise reduction techniques are widely adopted as a result of the application efficiency by absorption, reflection, or scattering the sound waves with acoustically engineered passive materials [6,7]. Such techniques are suitable for large-scale applications while lacking the ability for online monitoring of the noise level. In addition, the one-off nature of passive methods prevents their flexibility to handle prompt and localized noise sources. In recent decades, active noise control (ANC) techniques have been extensively researched to achieve real-time adaptation to variation in noise conditions [8–10], such as in active noise barrier applications [11] or noise reduction in vehicles [12] and headphones [13]. ANC systems introduce additional active loudspeakers, which are often referred to as “secondary

sources”, to generate canceling signals with similar amplitudes while opposite in phase to the noises. To date, ANC schemes mainly follow feedforward [14,15] and feedback [16,17] approaches. A single-channel feedforward system is the classic ANC algorithm consisting of a reference microphone to detect the noise to be canceled and an error microphone to monitor the system performance by detecting the residual error [8]. When sensing or estimating the target noise as the reference signal is not possible, the feedback approach is required in the ANC architecture. This paper mainly focuses on the feedforward approach for its robustness from straightforward environmental noise measurement. The key to feedforward ANC implementation is the effective estimation of the secondary path, which is understood as an adaptive filter to produce a phase-countering sound for the noise canceling at the error microphone. Currently, the most-preferred filter iteration technique is the filtered-x least mean square (FxLMS) algorithm [18] for its efficiency in computation and robustness for either single-channel or multi-channel applications [14,19,20].

Current ANC systems mainly use conventional voice coil loudspeakers (VCLs) as secondary sources. However, the omnidirectional nature of VCLs may induce adverse effects, such as the increment in the sound pressure level (SPL) in neighboring areas apart from the target position [21] and undesired acoustic feedback into the reference microphone [22]. Considering such issues from VCLs, a novel type of directional speaker termed parametric array loudspeaker (PAL) [23] has gained interest in ANC research. Due to nonlinear effects in acoustic wave propagation, low-frequency audible signals can be transmitted by ultrasound carrier waves through amplitude modulation (AM) techniques. PAL comprises multiple ultrasound transducers arranged in an array to project audio signals directionally based on the high directivity of carrier wave beams produced by limited aperture ultrasound arrays [24]. This facilitates localized ANC using PALs with minimal impact on non-interested sites, which has been validated in the literature [25].

Inspired by previous research, this paper explores the feasibility of localized monotone noise suppression with PALs embedded in a feedforward ANC system constructed with off-the-shelf, consumer-grade equipment. The algorithm is designed based on FxLMS architecture and solely implemented in software through a generic personal computer (PC). A customized hexagonal PAL functioned as the secondary source for the directional projection of monotone noise-countering signals. Experimental verification and comparison of noise reduction results are performed for the proposed method versus the results from using generic VCLs. The main contribution of the paper is summarized as follows:

- Demonstration of the enhanced directivity and operation distance for monotone noise suppression with PALs.
- Exploration of the feasibility of implementing the PAL-driven ANC system with a PC-powered platform and generic audio hardware.

The remaining paper is organized as follows. Section 2 describes the implemented FxLMS algorithm including offline secondary path identification and adaptive noise filter design. This section also briefly depicts the origination of the super-directivity of PALs. Section 3 discusses the realization of the PC-based ANC system. Section 4 presents the experimental characterization of PAL’s pressure field in terms of the directivity and axial pressure distribution. Section 5 describes the experimental evaluation of using the PAL for directional monotone noise suppression and provides comparisons against conventional VCLs to demonstrate the advantage of PALs in terms of operating distance and directivity. Section 6 concludes the paper and discusses the possible future improvements.

2. Theory and Methods

2.1. FxLMS Algorithm for Adaptive Noise Filter Design

The least mean squares (LMS) algorithms are based on the fundamental principles of Wiener filtering following the steepest gradient descent to produce optimized finite impulse response (FIR) filters. The FxLMS algorithm is an iterative adaptation of the LMS method and is now considered the baseline algorithm in ANC, known for its simplicity, low computational cost, and stable convergence [26]. Figure 1a shows a complete diagram

of the FxLMS algorithm for the single-channel noise reduction considered in this paper. One key element in the algorithm is determining the secondary path filter $\mathbf{s}(n)$, which depicts the acoustic path for the projection of counter-noise sound from the secondary source to the target where the error microphone locates. Neglecting the response from the secondary path can result in misjudgment of the optimum noise-canceling signal and affect the algorithm’s convergence [8]. Consider an adaptive FIR filter for the ANC control $\mathbf{w}(n)$; the residual noise measured at the error microphone $e(n)$ can be expressed as

$$e(n) = d(n) - [\mathbf{w}(n) \times x(n)] \times \mathbf{s}(n), \tag{1}$$

where $x(n)$ is the ambient noise signal and $d(n)$ is the measured ambient noise signal at the reference microphone through the primary path $\mathbf{p}(n)$. The LMS constraint requires the cost function $\zeta(n) = e^2(n)$ to be minimum by letting $\nabla \zeta(n)$ approach zero. Using the gradient descent method, the iteration for updating $\mathbf{w}(n)$ is expressed as

$$\mathbf{w}(n + 1) = \mathbf{w}(n) + \frac{\mu}{2} \nabla \zeta(n), \tag{2}$$

where μ is the filter learning rate to control the iteration step size. By derivation of $\nabla \zeta(n)$, the above iteration can be expanded as

$$\mathbf{w}(n + 1) = \mathbf{w}(n) - \mu e(n) \mathbf{s}(n) \times x(n). \tag{3}$$

Since $\mathbf{s}(n)$ is unknown, $\hat{\mathbf{s}}(n)$ is applied as a legitimate estimation of the secondary path. $x'(n)$ represents the output from $\hat{\mathbf{s}}(n)$ as

$$x'(n) = \hat{\mathbf{s}}(n) \times x(n), \tag{4}$$

which updates Equation (3) into

$$\mathbf{w}(n + 1) = \mathbf{w}(n) - \mu e(n) x'(n). \tag{5}$$

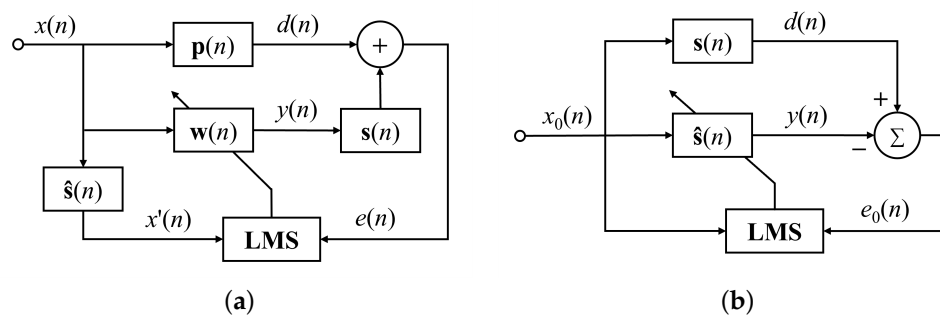


Figure 1. Block diagram of the implemented FxLMS algorithm with offline identification of the secondary path $\mathbf{s}(n)$. (a) The complete FxLMS algorithm, where $\mathbf{w}(n)$ is the adaptive ANC filter constrained by the estimated secondary path $\hat{\mathbf{s}}(n)$ and the residual error $e(n)$. (b) The offline identification of the secondary path for estimation of the LMS-constrained filter $\hat{\mathbf{s}}(n)$.

The aim of this paper is focused on the elimination of monotone noises, which can cause more harm to people’s mental health in modern urban or industrial environments. Hence, we adopt an offline approach to identify the secondary path for its straightforwardness in acquiring $\hat{\mathbf{s}}(n)$. The monotone noise features a concentrated power spectrum to represent an acoustic environment with its spectrum characteristic that does not change over time; so, we also use fixed step sizes in the algorithm for the iteration of the FIR filters. Since offline identification is performed as a standalone process, it does not introduce extra computation complexity into the main ANC algorithm to compromise its robustness. However, if environmental ambient noises such as Gaussian white noise are considered in ANC, the adaptive filter iteration step size should be considered due to the variation in

the noise power spectrum. To conclude, the complete FxLMS algorithm implemented in this paper can be summarized into two steps. The first step is the offline identification of the secondary path following the diagram shown in Figure 1b. By monitoring the ambient noise $x_0(n)$ and the residual error $e_0(n)$ at the target position, an LMS-constrained $\hat{s}(n)$ can be estimated. The second step is to update the adaptive filter $w(n)$ to achieve ANC following Equation (5) using $\hat{s}(n)$. As a result, signal $y(n)$ is computed from $\mathbf{w}(n)$ of a number of M taps as the driving signal for the secondary source as

$$y(n) = \sum_{i=0}^{M-1} w_i(n)x(n-i). \tag{6}$$

The practical system implementation will be described in detail in Sections 3 and 5.

2.2. PAL as the Directional Secondary Source

PAL can generate highly directional audible sound fields based on the nonlinear acoustic wave attenuation in air. In simple terms, for an acoustic beam containing multiple frequency components, as the wave propagates, the high-frequency contents attenuate faster to leave over the lowest frequency component as the subtraction result of the primary frequencies. Hence, it is possible to reproduce audible sound waves from high-frequency carrier waves through self-demodulation during propagation. The classic nonlinear acoustic model was derived by Khokhlov, Zabolotskaya, and Kuznetsov, known as the KZK equation, by considering the absorption of finite amplitude acoustic waves. In the far field, the derived quasilinear solution can predict the overall pressure distribution [27]. The resulting pressure field p is considered a combination of the solution to the linear ultrasound field p_1 and the nonlinear demodulated field result p_2 as $p = p_1 + p_2$. For a known ultrasound field, p_1 can be used as the driving source to solve for p_2 , and the KZK equation is converted into [28,29]

$$\frac{\partial^2 p_2}{\partial z \partial \tau} = \frac{c_0}{2} \nabla_r^2 p_2 + \frac{\delta}{2c_0^3} \frac{\partial^3 p_2}{\partial \tau^3} + \frac{\beta}{2\rho_0 c_0^3} \frac{\partial^2 p_1^2}{\partial \tau^2}. \tag{7}$$

This equation describes p_1 and p_2 's relation in the z -propagating axial direction, where $\tau = t - z/c_0$ is the retarded time, and δ and β are the diffusivity and coefficient of nonlinearity, respectively. $\nabla_r^2 = \partial^2/\partial r^2 + r^{-1}(\partial/\partial r)$, where r is the transverse radial coordinate in the xy plane. c_0 and ρ_0 are the sound velocity and density of the air medium, respectively. Berkta's solution of Equation (7) gives a simplified time-domain expression of the reproduced audio wave in the far field $p_2(r, z, \tau)$, which is proportional to the second derivative of the squared envelope through amplitude modulation (AM) of the primary wave $p_1(r, z, \tau)$ [30]. This is considered the foundation for implementing AM techniques for PALs [31,32]. For a primary ultrasound carrier wave of the angular frequency ω_c and initial amplitude P_0 , the AM-processed ultrasound pressure is [29]

$$p_1(r, z, \tau) = P_0 E(\tau) \sin(\omega_c \tau) e^{-\alpha z} H(a - r), \tag{8}$$

where $E(\tau)$ is the AM envelope of the primary wave. a is the radius of the source aperture and α is the absorption coefficient. $H(\cdot)$ is the unit step function. Hence, the self-demodulated audible wave can be expressed as [28,29,33]

$$p_2(r, z, \tau) \approx \frac{\beta P_0^2 a^2}{16\rho_0 c_0^4 z \alpha} \frac{\partial^2}{\partial \tau^2} E^2(\tau). \tag{9}$$

For a proof-of-principle study to explore PAL as the secondary ANC source, in this paper we choose a simple AM method using the double-sideband amplitude modulation

(DSBAM) technique [24]. For the target audio under modulation $g(\tau)$, the DSB modulated signal for PAL actuation is expressed as

$$g_{DSB}(\tau) = [1 + mg(\tau)] \sin(\omega_c \tau), \tag{10}$$

where $0 < m \leq 1$ is the modulation index.

3. Realization of the PC-Powered ANC System

The proposed ANC system is developed on a generic PC architecture utilizing standard PC-integrated hardware as the signal processing and noise control platform. The PC has a quad-core CPU (Core i7-7700, Intel, CA, USA) and 16 GB RAM. Other peripheral sensors and components are generic audio hardware such as microphones, sound cards, and audio power amplifiers (PAs). The closed-loop noise sampling hardware includes two condenser microphones (ECM8000, Behringer, Germany) with a high dynamic range as the reference and error sensors, respectively. A high-precision, fast-rate, multichannel sound card (UMC404HD, Behringer, Germany) is used for signal digitizing. Both conventional VCL and bespoke PAL are tested and compared as secondary sources. A high-bit-depth oscilloscope provides real-time monitoring of the noise reduction results.

Figure 2 shows the system diagram to implement the FxLMS algorithm for real-time ANC. The PC interfaces with the sound card to process the audio data input/output (I/O) streaming, as well as the main ANC computation. The I/O audio signals are streamed and buffered in segments by 2048 samples per frame through the USB interface from the sound card into the PC via standard audio driver types such as ASIO. The multichannel sound card digitizes the noise data at a bit rate of 44.1 kHz and a bit depth of 16 bit for fast-rate, high-precision sampling. Real-time audio data processing is implemented with a PC-based software environment to run the FxLMS algorithm by reading the data from the Audio Data Read module and provides the ANC signal to drive the secondary loudspeaker from the Audio Data Write module, as shown in the block diagram of Figure 2. The FxLMS computation and I/O streaming of the processed data are all executed in segments of the same length following the same sampling rate.

According to the proposed FxLMS block diagram in Section 2, the first step is to estimate the secondary path following Figure 1b using white noise. The secondary path filter $\hat{s}(n)$ is recorded until the convergence error reaches -40 dB. The FxLMS algorithm is then executed with the saved $\hat{s}(n)$ following the process in Figure 1a. When using PAL as the secondary source, the speaker instrumentation is more complex than the VCL case. The PAL hardware includes a bespoke PAL constructed with an array of transducers, which is powered by a PA module associated with a generic signal generator for DSB modulation of the actuation signals.

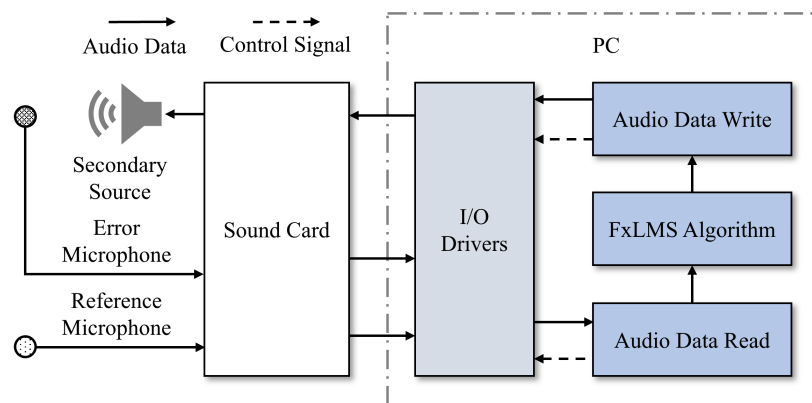


Figure 2. System diagram of the PC-powered ANC system implemented with the FxLMS algorithm.

4. Experimental Characterization of PAL's Pressure Field

4.1. Characterization of PAL's Directivity

VCLs have a nearly omnidirectional directivity, while PALs can achieve a narrower directivity in the far field following the beam width defined by the ultrasound carrier wave [24,29]. The PAL under test is shown in Figure 3a, which consists of 198 pieces of 40 kHz, 10 mm diameter, airborne ultrasound transducers (KS-A1040H07CTR, Kesen, Guangdong, China) arranged in a hexagon-shaped array with an aperture size of 17 cm in diameter. Theoretically, the demodulated audio beam directivity $D(\theta)$ can be predicted by the main lobe determined by the proposed array aperture of L and wave number of k as [34]

$$D(\theta) = \text{sinc} \left| \frac{kL \sin \theta}{2} \right|. \quad (11)$$

To verify the PAL spatial characteristics, we measured the array far-field directivity at a distance of 1 m away from the aperture, using both the microphone and a calibrated sound level meter (AS844+, HIMA Instrument, Hong Kong, China) when the PAL is driven with a 1 kHz modulated continuous wave signal. The microphone senses pressure levels in the test field by recording peak-to-peak voltages, which are then converted into decibels (dBs) by post-processing. The sound level meter directly records the pressure levels in dB by A-weighting to simulate the human auditory characteristics. The measurement is conducted by mounting the test source on a rotary stage and manually rotating the source to record the data at every 5° step size. The comparison of the two measurement approaches is presented in Figure 3b, indicating that both measurement methods give a similar plot to clearly depict the PAL's far-field directivity, showing a −3 dB main lobe width of around 40°. The form factor of the adopted PAL also gives rise to two grating lobes at ±30° with lower amplitudes compared with the main lobe [24,34].

The directivities of the PAL with an aperture size of 17 cm and a generic VCL with a sound emitting surface area of 85 mm × 70 mm are measured with the sound level meter at the same 100 cm distance when both emitting a 1 kHz signal. The comparison is shown in Figure 3c by plotting both directivity maps with the normalized amplitude (n.a.). The VCL presents a wide directivity that is close to an omnidirectional pattern, with a −3 dB beam width of around 110°, while the PAL's −3 dB beam width is reduced to around 40° by considering the main lobes. Hence, for the current aperture design shown in Figure 3a, as the secondary source, the PAL can reduce the effective beam width by 64% of that of the conventional loudspeaker to provide much more directional ANC effects.

Figure 3d further compares the directivity pattern of beams projected from the PAL when the carrier waves are modulated with different audio frequencies. For verification purposes, the test frequencies are selected from low to high at 250 Hz, 1 kHz, and 4 kHz, within the transducer's −6 dB bandwidth of around 3 kHz. The results demonstrate similar beam directivity patterns when the PAL is driven with signals modulated with either low or high audio frequencies. This further verifies the feasibility of using the PAL to tackle different monotone noises.

4.2. Characterization of PAL's Axial Pressure

Apart from the directivity characterization, we further examine and compare the axial pressure distribution of the PAL against traditional VCL. Due to the non-linear nature during the propagation of parametric acoustic beams, the self-demodulated audible frequency beam can be considered as an end-fire array created along the directivity of the primary beam defined by the carrier frequency wave [25]. Hence, this confinement from the carrier wave may mitigate the attenuation of the resultant audible signal. To evaluate this, we characterize both the PAL and VCL by measuring the attenuated sound levels in dB using the sound level meter along the axial direction. The measurement and comparison results are shown in Figure 4. For both the PAL and VCL, the audible signal of interest is 1 kHz with the initial sound pressure at the source surface calibrated as 90 dB. Then, the SPL is recorded at every 20 cm step away from the source in a range of 0~300 cm. The

measurements indicate that the PAL attenuates less and gives a 20 dB higher SPL value than the VCL at various distances on average. This result further verifies PAL's advantage as the secondary source for ANC to provide the possibility of long-distance operation.

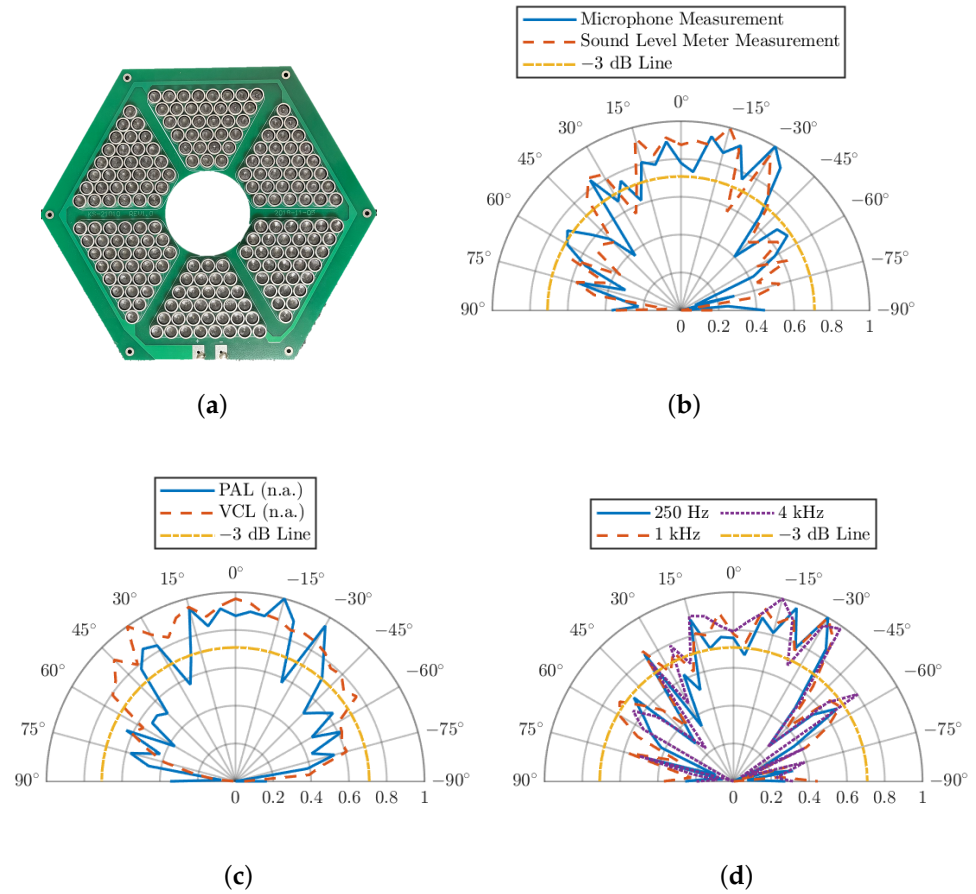


Figure 3. Experimental examination of the PAL's directivity in the far field of 1 m away from the source. (a) The PAL constructed with ultrasound transducers. (b) Comparison of the measurements by using the condensed microphone and the sound level meter. (c) Comparison of the normalized amplitudes showing directivities of the PAL and conventional VCL measured by the sound level meter. (d) The directivities of the demodulated audio beams of different frequencies.

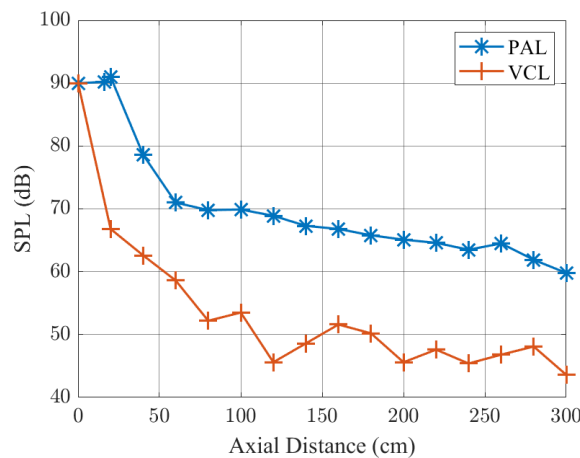
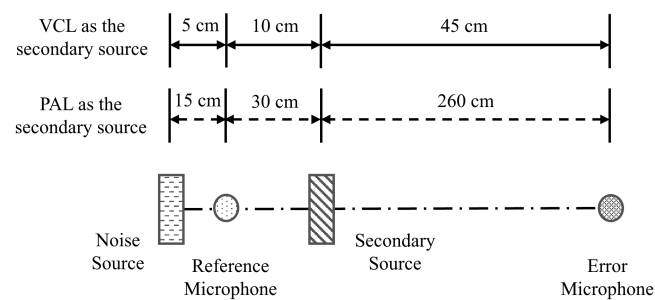


Figure 4. Comparison of measured axial sound attenuation characteristics of the PAL against VCL when projecting 1 kHz audible signal with 90 dB initial SPL at the source surface.

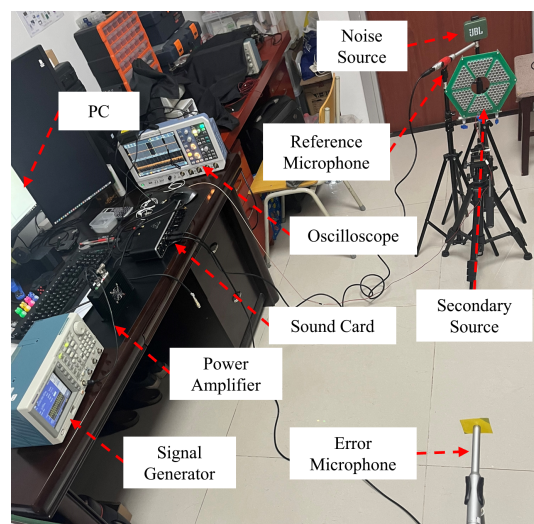
5. Experimental Evaluation for Directional Monotone Noise Suppression with PALs

5.1. Experimental Setup

We performed practical ANC experiments to examine the effectiveness of the implementation of PALs for long-distance localized monotone noise suppression. The schematic for the experimental setups is shown in Figure 5a and a photograph of the practical setup is shown in Figure 5b. A generic loudspeaker functions as the noise source at the far end of the entire scene to provide ambient monotone noise for suppression. Either PAL or VCL, as discussed in Section 3, is implemented as the secondary source. A reference microphone is placed close to the noise source to sample the ambient noise and an error microphone is placed at the location of interest to monitor the real-time residual noise. For comparison purposes, as shown in Figure 5a, the error microphone is placed at 260 cm away from the PAL, which is 5.8 times further compared with the case when using VCL as the secondary source. The practical setup illustration in Figure 5b shows the experimental scene, in which the PC functions as the core to process ANC algorithms and data I/O streaming. The real-time residual noise is collected by the error microphone at the location of interest and digitized via the sound card to be streamed to the PC. A high-precision oscilloscope also monitors the residual noises. The signal generator modulates the PC streamed secondary source driving signal in real-time with the transducer carrier frequency of 40 kHz to power the PAL via the PA module. For verification purposes, the test monotone noise was selected as 1 kHz in the experiments.



(a)



(b)

Figure 5. Experimental setup for the evaluation of the PAL for monotone noise suppression. (a) The schematic of the overall ANC scene using either PAL or VCL as the secondary source. (b) A photograph that illustrates the practical setup.

5.2. Evaluation of PAL for Directional Monotone Noise Suppression

As described in Section 2, the proposed ANC method requires an offline identification of the secondary path as the first step. Hence, the secondary path filters $\hat{s}(n)$ from using either VCL or PAL are measured with white noise following Figure 1b in the setups illustrated in Figure 5. This estimated $\hat{s}(n)$ is further embedded in the complete FxLMS algorithm to update the ANC control filter $\mathbf{w}(n)$. In our implementation, both filters have a tap number of 128, and the optimum filter learning rate is selected as 10^{-2} and 10^{-4} for the VCL and PAL cases, respectively, as concluded from repeated tests.

For a monotone noise of 1 kHz under test, the ANC results from using both VCL and PAL are analyzed with frequency spectra, as presented in Figure 6. The results show that either VCL or PAL can perform effective reduction of the monotone noise through the PC-powered ANC platform. At the frequency of 1 kHz, the noise level is suppressed by 14 dB in the VCL case and 8 dB in the PAL case. However, in the PAL case, the secondary path is 5.8 times longer than the VCL, which verifies the effectiveness of using PAL to achieve comparable noise reduction while at a much further distance. In Figure 6b, an extra frequency component at 2 kHz appears when the ANC is active. This undesired effect can be attributed to the harmonics distortion introduced by the bandwidth-limited transducers driven by signals modulated with simple DSBAM techniques, which can be further eliminated by using more elaborate AM methods [24,33,35].

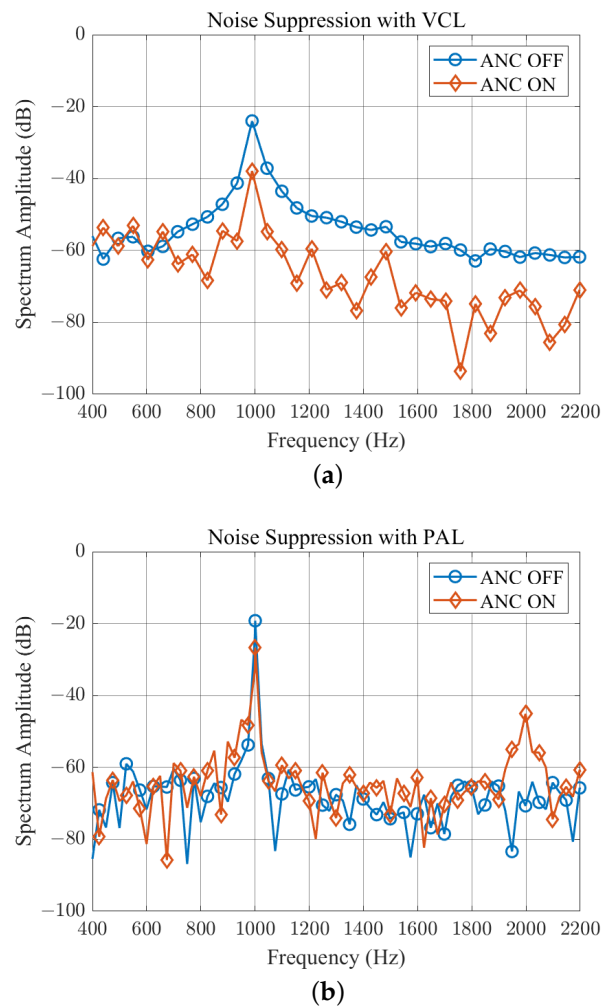


Figure 6. Measurement of 1 kHz monotone noise suppression results with (a) VCL or (b) PAL as the secondary source in the ANC system.

To confirm the directional noise suppression by using PAL, we further measured the practical noise reduction level along a horizontal range of 80 cm while keeping a constant perpendicular distance of 60 cm between the source plane and the measured plane where the error microphones are located, as shown in Figure 7a. We also used 1 kHz monotone noise for the test. The original and residual noises are measured for either the VCL or PAL case, and the noise attenuation levels are calculated as summarized in Figure 7b. For both the VCL and PAL cases, the maximum noise attenuation level appears at 0° along the normal axis of the secondary source's surface with values of 10.7 dB and 7.6 dB for the VCL and PAL cases, respectively. This measurement correlates with the spectra analysis in Figure 6. The directivity characteristics of different loudspeakers in noise suppression can be concluded by analyzing the 6 dB ANC range. In the VCL case, the 6 dB ANC range covers a horizontal distance of around 44 cm, which is reduced to 20 cm when using the PAL. This result also cross-validates with Figure 3 to confirm PAL's advantage of narrower directivity for targeting localized noise sources.

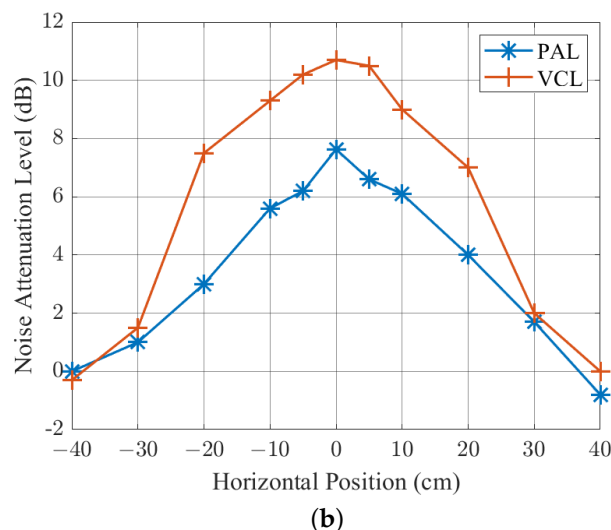
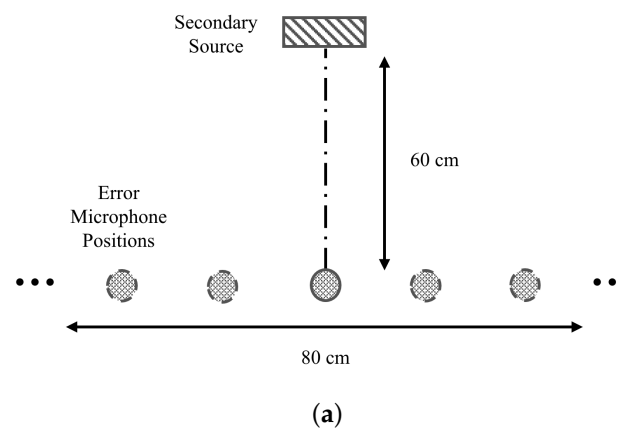


Figure 7. Measured noise attenuation levels across a horizontal spatial range of 80 cm at the same distances between the secondary source and the error microphone for the VCL and PAL cases. (a) Schematic of the setup. (b) Comparison of measured results.

6. Conclusions and Future Work

This paper explores and confirms the feasibility of using PALs as the secondary source for directional monotone noise suppression at long distances by proposing a PC-powered ANC system running adaptive noise reduction algorithms. The proposed system is constructed with the conventional PC and generic audio hardware to provide a cost-

effective ANC platform. For the PAL with an aperture of 17 cm working at 40 kHz carrier frequency, the proposed ANC system can achieve around 8 dB suppression of monotone noises 260 cm away from the target location. Experimental measurements and comparisons confirm the advantages of PALs over conventional VCLs in long-range directional ANC by reducing the -3 dB effective beam width by around 64% to enhance the directivity while extending the operation distance by 5.8 times when a similar ANC result is achieved.

Future improvements of the proposed directional ANC solution include three aspects such as the PAL array, ANC algorithm, and system development. The future PAL design will consider the optimization of the array geometry to reduce the interference of the grating lobes by using narrower array element spacing or a curved aperture. In addition, considering the harmonic aliasing effects in PALs, more elaborate signal modulation techniques will be explored and integrated into the proposed ANC scheme to further restrain the higher harmonics. The current system employs offline identification of the secondary path, which requires fixed positions of the target area and the PAL as well as quasi-static noise conditions, limiting the system's flexibility. This can be further improved by introducing more elaborate ANC algorithms considering online estimation of the secondary path, also targeting diverse noise types such as white, pink, or pulsed noises. During experiments, we observed that it is crucial to define the proper system buffer size for data streaming and processing in the PC-based algorithm to balance the real-time requirement and convergence of the residual noise. Hence, although more costly, high-speed hardware such as digital signal processors (DSPs) or field-programmable gate arrays (FPGAs) will be considered to improve the real-time characteristics of the current system.

Author Contributions: Conceptualization, H.W., J.Z. and L.G.; data curation, H.W. and J.Z.; formal analysis, H.W. and J.Z.; funding acquisition, H.W.; investigation, H.W., J.Z. and L.G.; methodology, H.W., J.Z. and L.G.; resources, H.W. and L.G.; software, H.W. and J.Z.; supervision, H.W. and Y.L.; visualization, H.W. and J.Z.; writing—original draft, H.W. and J.Z.; writing—review and editing, H.W., L.G. and Y.L. All authors have read and agreed to the published version of the manuscript.

Funding: This work is supported by the Natural Science Foundation of Tianjin (No. 22JCZDJC00270).

Data Availability Statement: The data presented in this study are available on request from the corresponding author.

Conflicts of Interest: The authors declare no conflict of interest.

References

1. Basner, M.; Babisch, W.; Davis, A.; Brink, M.; Clark, C.; Janssen, S.; Stansfeld, S. Auditory and non-auditory effects of noise on health. *Lancet* **2014**, *383*, 1325–1332. [[CrossRef](#)] [[PubMed](#)]
2. Lie, A.; Skogstad, M.; Johannessen, H.A.; Tynes, T.; Mehlum, I.S.; Nordby, K.C.; Engdahl, B.; Tambs, K. Occupational noise exposure and hearing: A systematic review. *Int. Arch. Occup. Environ. Health* **2016**, *89*, 351–372. [[CrossRef](#)] [[PubMed](#)]
3. Münzel, T.; Sørensen, M.; Daiber, A. Transportation noise pollution and cardiovascular disease. *Nat. Rev. Cardiol.* **2021**, *18*, 619–636. [[CrossRef](#)]
4. Clark, C.; Crumpler, C.; Notley, H. Evidence for Environmental Noise Effects on Health for the United Kingdom Policy Context: A Systematic Review of the Effects of Environmental Noise on Mental Health, Wellbeing, Quality of Life, Cancer, Dementia, Birth, Reproductive Outcomes, and Cognition. *Int. J. Environ. Res. Public Health* **2020**, *17*, 393. [[CrossRef](#)]
5. De Ridder, D.; Schlee, W.; Vanneste, S.; Londero, A.; Weisz, N.; Kleinjung, T.; Shekhawat, G.S.; Elgoyhen, A.B.; Song, J.J.; Andersson, G.; et al. Tinnitus and tinnitus disorder: Theoretical and operational definitions (an international multidisciplinary proposal). *Prog. Brain Res.* **2021**, *260*, 1–25. [[PubMed](#)]
6. Pelat, A.; Gautier, F.; Conlon, S.C.; Semperlotti, F. The acoustic black hole: A review of theory and applications. *J. Sound Vib.* **2020**, *476*, 115316. [[CrossRef](#)]
7. Gao, N.; Zhang, Z.; Deng, J.; Guo, X.; Cheng, B.; Hou, H. Acoustic Metamaterials for Noise Reduction: A Review. *Adv. Mater. Technol.* **2022**, *7*, 2100698. [[CrossRef](#)]
8. Kuo, S.; Morgan, D. Active noise control: A tutorial review. *Proc. IEEE* **1999**, *87*, 943–975. [[CrossRef](#)]
9. George, N.V.; Panda, G. Advances in active noise control: A survey, with emphasis on recent nonlinear techniques. *Signal Process.* **2013**, *93*, 363–377. [[CrossRef](#)]
10. Lu, L.; Yin, K.L.; de Lamare, R.C.; Zheng, Z.; Yu, Y.; Yang, X.; Chen, B. A survey on active noise control in the past decade—Part I: Linear systems. *Signal Process.* **2021**, *183*, 108039. [[CrossRef](#)]

11. Sohrabi, S.; Pàmies Gómez, T.; Romeu Garbí, J. Proper location of the transducers for an active noise barrier. *J. Vib. Control* **2023**, *29*, 2290–2300. [[CrossRef](#)]
12. Jiang, Y.; Chen, S.; Gu, F.; Meng, H.; Cao, Y. A modified feedforward hybrid active noise control system for vehicle. *Appl. Acoust.* **2021**, *175*, 107816. [[CrossRef](#)]
13. Ang, L.Y.L.; Koh, Y.K.; Lee, H.P. The performance of active noise-canceling headphones in different noise environments. *Appl. Acoust.* **2017**, *122*, 16–22. [[CrossRef](#)]
14. Aslam, M.S.; Shi, P.; Lim, C.C. Robust Active Noise Control Design by Optimal Weighted Least Squares Approach. *IEEE Trans. Circuits Syst. I Regul. Pap.* **2019**, *66*, 3955–3967. [[CrossRef](#)]
15. Airimitoai, T.B.; Landau, I.D.; Melendez, R.; Dugard, L. Algorithms for Adaptive Feedforward Noise Attenuation—A Unified Approach and Experimental Evaluation. *IEEE Trans. Control Syst. Technol.* **2021**, *29*, 1850–1862. [[CrossRef](#)]
16. Akhtar, M.T.; Mitsuhashi, W. Improving Performance of Hybrid Active Noise Control Systems for Uncorrelated Narrowband Disturbances. *IEEE Trans. Audio Speech Lang. Process.* **2011**, *19*, 2058–2066. [[CrossRef](#)]
17. Xie, X.; Shi, X.; Chen, Y. A feedforward and feedback composite active noise reduction headset based on inverse filter frequency equalization and its DSP system implementation. *Appl. Acoust.* **2023**, *202*, 109151. [[CrossRef](#)]
18. Morgan, D.R. History, applications, and subsequent development of the FXLMS Algorithm [DSP History]. *IEEE Signal Process. Mag.* **2013**, *30*, 172–176. [[CrossRef](#)]
19. Yang, F.; Guo, J.; Yang, J. Stochastic Analysis of the Filtered-x LMS Algorithm for Active Noise Control. *IEEE/ACM Trans. Audio Speech Lang. Process.* **2020**, *28*, 2252–2266. [[CrossRef](#)]
20. Dimino, I.; Colangeli, C.; Cuenca, J.; Vitiello, P.; Barbarino, M. Active Noise Control for Aircraft Cabin Seats. *Appl. Sci.* **2022**, *12*, 5610. [[CrossRef](#)]
21. Aslan, F.; Paurobally, R. Modelling and simulation of active noise control in a small room. *J. Vib. Control* **2018**, *24*, 607–618. [[CrossRef](#)]
22. Aslam, M.S.; Shi, P.; Lim, C.C. Self-adapting variable step size strategies for active noise control systems with acoustic feedback. *Automatica* **2021**, *123*, 109354. [[CrossRef](#)]
23. Bennett, M.B.; Blackstock, D.T. Parametric array in air. *J. Acoust. Soc. Am.* **1975**, *57*, 562–568. [[CrossRef](#)]
24. Wang, H.; Tang, J.; Wu, Z.; Liu, Y. A Multi-beam Steerable Parametric Array Loudspeaker for Distinct Audio Content Directing. *IEEE Sens. J.* **2022**, *22*, 13640–13647. [[CrossRef](#)]
25. Gan, W.S.; Yang, J.; Kamakura, T. A review of parametric acoustic array in air. *Appl. Acoust.* **2012**, *73*, 1211–1219. [[CrossRef](#)]
26. Burgess, J.C. Active adaptive sound control in a duct: A computer simulation. *J. Acoust. Soc. Am.* **1981**, *70*, 715–726. [[CrossRef](#)]
27. Westervelt, P.J. Parametric Acoustic Array. *J. Acoust. Soc. Am.* **1963**, *35*, 535–537. [[CrossRef](#)]
28. Averkiou, M.A.; Lee, Y.; Hamilton, M.F. Self-demodulation of amplitude- and frequency-modulated pulses in a thermoviscous fluid. *J. Acoust. Soc. Am.* **1993**, *94*, 2876–2883. [[CrossRef](#)]
29. Pompei, F.J. Sound From Ultrasound: The Parametric Array as an Audible Sound Source. Ph.D. Thesis, Massachusetts Institute of Technology, Cambridge, MA, USA, 2002.
30. Berktaý, H. Possible exploitation of non-linear acoustics in underwater transmitting applications. *J. Sound Vib.* **1965**, *2*, 435–461. [[CrossRef](#)]
31. Shi, C.; Kajikawa, Y. Volterra model of the parametric array loudspeaker operating at ultrasonic frequencies. *J. Acoust. Soc. Am.* **2016**, *140*, 3643–3650. [[CrossRef](#)]
32. Zhong, J.; Kirby, R.; Qiu, X. The near field, Westervelt far field, and inverse-law far field of the audio sound generated by parametric array loudspeakers. *J. Acoust. Soc. Am.* **2021**, *149*, 1524–1535. [[CrossRef](#)] [[PubMed](#)]
33. Tan, E.L.; Ji, P.; Gan, W.S. On preprocessing techniques for bandlimited parametric loudspeakers. *Appl. Acoust.* **2010**, *71*, 486–492. [[CrossRef](#)]
34. Schmerr, L.W., Jr. Phased array beam modeling (1-D elements). In *Fundamentals of Ultrasound Phased Arrays*; Springer International Publishing: Cham, Switzerland, 2015; Chapter 4, pp. 73–98.
35. San Martín, R.; Tello, P.; Valencia, A.; Marzo, A. Experimental Evaluation of Distortion in Amplitude Modulation Techniques for Parametric Loudspeakers. *Appl. Sci.* **2020**, *10*, 2070. [[CrossRef](#)]

Disclaimer/Publisher’s Note: The statements, opinions and data contained in all publications are solely those of the individual author(s) and contributor(s) and not of MDPI and/or the editor(s). MDPI and/or the editor(s) disclaim responsibility for any injury to people or property resulting from any ideas, methods, instructions or products referred to in the content.